NANO · MICRO small
www.small-journal.com

Insights into Electrolytic Pre-Lithiation: A Thorough Analysis Using Silicon Thin Film Anodes

Lukas Haneke, Felix Pfeiffer, Peer Bärmann, Jens Wrogemann, Christoph Peschel, Jonas Neumann, Fabian Kux, Sascha Nowak, Martin Winter, and Tobias Placke**

Pre-lithiation via electrolysis, herein defined as electrolytic pre-lithiation, using cost-efficient electrolytes based on lithium chloride (LiCl), is successfully demonstrated as a proof-of-concept for enabling lithium-ion battery full-cells with high silicon content negative electrodes. An electrolyte for pre-lithiation based on γ-butyrolactone and LiCl is optimized using boron-containing additives (lithium bis(oxalato)borate, lithium difluoro(oxalate) borate) and CO_2 with respect to the formation of a protective solid electrolyte interphase (SEI) on silicon thin films as model electrodes. Reversible lithiation in Si||Li metal cells is demonstrated with Coulombic efficiencies (C_{Eff}) of 95–96% for optimized electrolytes comparable to 1 M $LiPF_6$/EC:EMC 3:7. Formation of an effective SEI is shown by cyclic voltammetry and X-ray photoelectron spectroscopy (XPS). electrolytic pre-lithiation experiments show that notable amounts of the gaseous product Cl_2 dissolve in the electrolyte leading to a self-discharge Cl_2/Cl^- shuttle mechanism between the electrodes lowering pre-lithiation efficiency and causing current collector corrosion. However, no significant degradation of the Si active material and the SEI due to contact with elemental chlorine is found by SEM, impedance, and XPS. In NCM111||Si full-cells, the capacity retention in the 100th cycle can be significantly increased from 54% to 78% by electrolytic pre-lithiation, compared to reference cells without pre-lithiation of Si.

1. Introduction

Recently, electric mobility and the use of lithium-ion batteries (LIBs) as energy storage technology for automotives have crystallized as the most-promising, energy-efficient alternative to combustion engines vehicles with the potential to drastically reduce the emission of carbon dioxide and air pollution by toxic exhaust fumes.[1] The demand for increased energy density while achieving sufficient fast charging capability and long cycle life remains one of the main challenges for wide-range application and mass market penetration of battery-driven propulsion. One strategy to increase the energy density of LIBs on the cell level is to improve the negative electrode's specific capacity. Silicon (Si) has been investigated thoroughly as an active material for the negative electrode (anode) during the past decades due to its high theoretical capacity of 3579 mAh g^{-1} ($Li_{15}Si_4$) and low average de-lithiation potential (≈0.4 V vs Li|Li^+).[2–4] Despite that, pure Si suffers from its high volume expansion of ≈300% upon lithiation leading to capacity loss by particle cracking and continuous formation of the solid electrolyte interphase (SEI).[5–7] Several strategies have been adopted to improve the electrochemical stability and reversibility of (de-)lithiation for Si electrodes, such as nano-sizing Si particles,[8,9] use of composites with graphitic and non-graphitic carbons,[10] use of silicon dioxide,[11] or intermetallics (e.g., with iron such as Fe_xSi_y),[12,13] forming different electrochemically active or inactive matrices to buffer the Si expansion. Further, effective SEI formation and passivation were tailored using electrolyte additives, such as vinylene carbonate (VC), fluoroethylene carbonate (FEC),[14] or polymerizing additives, based on, for example, isocyanates or the in situ formation of CO_2.[15,16]

Although improvements in the cycle life of Si electrodes were reported in numerous publications with well-optimized, specifically structured, or alloyed active materials,[13,17] loss of active lithium during the first and ongoing charge/discharge cycles is still the major reason inhibiting the replacement of graphite as state-of-the-art (SOTA) LIB anode.[2,18,19]

Pre-lithiation has been widely applied on a laboratory scale to counteract the loss of active lithium, and impede capacity

L. Haneke, J. Wrogemann, C. Peschel, J. Neumann, F. Kux, S. Nowak, M. Winter, T. Placke
University of Münster
MEET Battery Research Center
Institute of Physical Chemistry
Corrensstraße 46 48149, Münster, Germany
E-mail: m.winter@fz-juelich.de; tobias.placke@uni-muenster.de
F. Pfeiffer, M. Winter
Helmholtz Institute Münster
IEK-12
Forschungszentrum Jülich GmbH
Corrensstraße 46 48149, Münster, Germany
P. Bärmann
Helmholtz-Zentrum Berlin für Materialien und Energie GmbH (HZB)
Albert-Einstein-Straße 15 12489, Berlin, Germany
The ORCID identification number(s) for the author(s) of this article can be found under https://doi.org/10.1002/smll.202206092.

DOI: 10.1002/smll.202206092

loss of LIB full -cells containing Si-based anodes.[18,20,21] Some methods aim at "over-lithiation" of positive electrode (cathode) active materials or sacrificial species as oxalates for the cathode leading to additional lithiation during the first charge in LIB full-cells.[22] While the addition of sacrificial salts might be included in the conventional manufacturing process, only small degrees of pre-lithiation (DoP) can be achieved, and this approach introduces further challenges as either inactive material is added or structural degradation of the cathode after the decomposition of sacrificial salts may arise. For direct pre-lithiation of the anode, three major approaches have been developed: i) chemical pre-lithiation has been conducted by immersion of graphite or Si-based electrodes into reducing solutions, for example, containing *n*-butyl lithium (*n*-BuLi), lithium naphthalene complexes,[23] or biphenyl-lithium complexes and other fluorinated aromatic hydrocarbon-lithium complex solutions with lower redox potentials enabling lithiation of the anode.[24] On the one hand, this strategy provides simple processability leading to efficient pre-lithiation, however, on the other hand, highly reactive and toxic reagents have to be handled under a strict inert atmosphere, which may bear safety issues and cause anode degradation.[20] ii) Pre-lithiation with Li metal foil or powder brought into direct contact on top of the anode[25] features a simple preparation at the expense of low control of the DoP, an increased inhomogeneity of lithiation and SEI formation, and potential safety issues in the case of pure metallic lithium as the pre-lithiation agent.[26] Stabilized or passivated lithium metal powder may be handled in a dry air atmosphere, however, safety remains a major challenge due to the high surface area of the powder.[27] Recent contact pre-lithiation concepts focus on the application of precisely dosed lithium metal by, for example, sputtering or chemical vapor deposition.[28] iii) Electrochemical pre-lithiation using Li metal as a counter electrode (CE) allows high controllability and homogeneity of lithiation, as the DoP, current density, and electrode/cell geometry can be adjusted accurately.[29] The additional processing step, costs of pure lithium metal, and related safety issues are disadvantages for industrial production, although commercial application exists for the production of pre-lithiated lithium-ion capacitors.[30]

This work focuses on another approach for electrochemical pre-lithiation, that is, electrolysis of an electrolyte salt, herein defined as electrolytic pre-lithiation (**Figure 1**).

While electrolytic pre-lithiation may exhibit similar advantages to "classical" electrochemical pre-lithiation as precise control over the DoP, costs and safety risks can be reduced by the use of inexpensive lithium salts or sacrificial electrodes instead of Li metal. However, scientific literature on electrolytic pre-lithiation is scarce so far. One study described pre-lithiation with a two-compartment cell setup using Cu as a sacrificial anode with an aqueous Li_2SO_4-based electrolyte separated from the cathodic half-cell containing an organic carbonate electrolyte by a LISICON membrane.[31] In general, lithium chloride (LiCl) is an appealing electrolyte salt due to its low cost and formation of gaseous chlorine upon oxidation of chloride anions. A roll-to-roll process using LiCl and γ-butyrolactone (GBL) as a solvent to pre-lithiate single and double-sided electrodes in an electrochemical bath was described in patents.[32,33]

With the possibility to not only compensate for the loss of active lithium in the 1st charge/discharge cycle but also in consecutive cycles by creating a "reservoir" of electrochemically active lithium within the negative electrode, LIB full-cells based on Si-materials with capacity retentions suitable for practical applications may be enabled by pre-lithiation. Using an optimized Si-alloy with a high first cycle Coulombic efficiency (C_{Eff}) of ≈87% as negative electrode active material, and pre-lithiation beyond compensation of the initial Li-loss to achieve a Li-reservoir, high capacity retention of 80% after ≈500 cycles could be shown for LIB full-cells.[34] By tailoring the DoP and the capacity balancing of negative to positive electrodes in full-cells (N/P ratio), the energy density and/or the cycle life of full-cells may be tuned.[34] For high DoPs and thus higher N/P ratios considering that Li-plating has to be impeded, a higher C_{Eff} was observed for pre-lithiated Si/C full-cells compared to non-pre-lithiated ones, even after the Li-reservoir was consumed.[34,35]

Herein, electrolytic pre-lithiation using LiCl and GBL is thoroughly investigated for Si thin film model electrodes with a thickness of ≈1 µm. Due to a lack of data regarding the impact of LiCl and the inferior SEI-forming ability of GBL,[36]

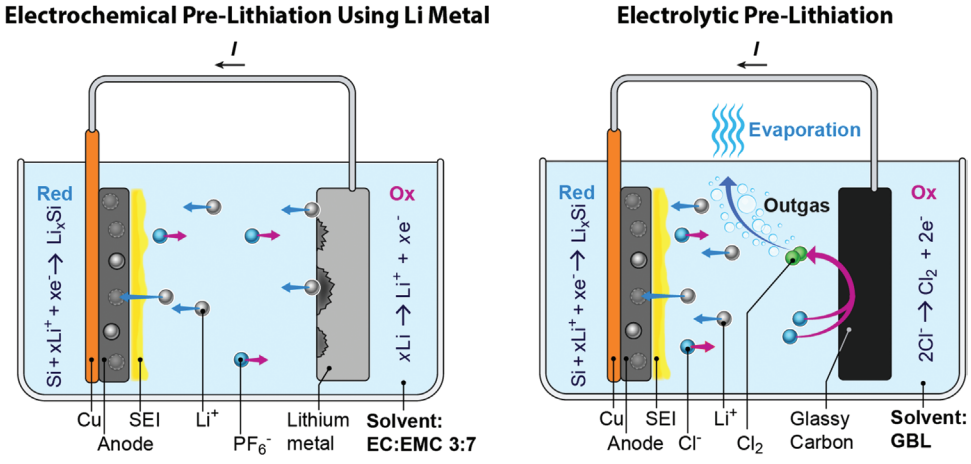

Figure 1. Schematic illustration of electrochemical pre-lithiation using lithium metal as a sacrificial electrode (left), and electrolytic pre-lithiation based on the oxidation of the electrolyte salt anions (here: Cl^-) as electron source (right).

electrolyte additives (e.g., VC and FEC) will be applied to enable effective SEI formation. CO_2 has been reported as an effective additive for lithium metal and Si-based electrodes,[37] and was reported as a potential pre-lithiation additive and solubility enhancer for LiCl in GBL.[33] Apart from that, boron-based salts, such as lithium bis(oxalato)borate (LiBOB) or lithium difluoro(oxalate)borate (LidFOB) were successfully applied as SEI-forming agents and conducting salts for graphite- or silicon-based LIB cells, in particular with alternative solvents such as propylene carbonate (PC) or GBL.[38–40]

Safety concerns, high costs, and extra processing time have hindered the large-scale application of pre-lithiation for LIB applications so far. The aim of this study is to shed light on electrolytic pre-lithiation with an emphasis on formed interphase (SEI) structures. Si thin films were used as a binder- and carbon-free model compound to facilitate analysis of the SEI and pave the path for future application of the pre-lithiation method to practical silicon/graphite composites with high Si content.

2. Results and Discussion

The first part of the results section focuses on the characterization of suitable electrolyte formulations enabling effective electrolytic pre-lithiation, which are based on lithium chloride as a salt/lithium source. Their electrochemical characteristics are investigated using Si thin films, which are combined with a spectroscopic SEI analysis. The application in a practical electrolytic pre-lithiation cell setup is subsequently evaluated. Mechanistic insights, the potential impact of the process on electrode kinetics, as well as the SEI, and verification of the pre-lithiation method via analysis of LIB full-cells are described in the following parts.

2.1. Electrolyte Characterization in Si||Li Metal Cells and SEI Analysis

The main redox reactions during pre-lithiation of silicon thin films via electrolysis of LiCl as a lithium source can be stated as follows

$$\text{Cathodic reaction}: \mathrm{Si} + x\mathrm{Li}^+ + x\mathrm{e}^- \rightleftharpoons \mathrm{Li}_x\mathrm{Si} \quad (1)$$

$$\text{Anodic reaction}: x\mathrm{Cl}^- \rightleftharpoons \frac{x}{2}\mathrm{Cl}_2 + x\mathrm{e}^- \quad (2)$$

Due to the low solubility of LiCl in SOTA organic carbonate solvents, such as dimethyl carbonate (DMC), ethyl methyl carbonate (EMC), or PC, different solvents have been evaluated to achieve a sufficiently high solubility. Providing an acceptable solubility and ionic conductivity, GBL was selected as the solvent of choice (Table S1, Supporting Information).

To characterize the general reversibility of (de-)lithiation of silicon and to obtain information about the passivation behavior, 0.7 M LiCl in GBL (=baseline electrolyte; BL) was evaluated in Si||Li metal cells, and compared to a SOTA LIB electrolyte 1 M $LiPF_6$ in EC:EMC 3:7 by wt. (**Figure 2**a).

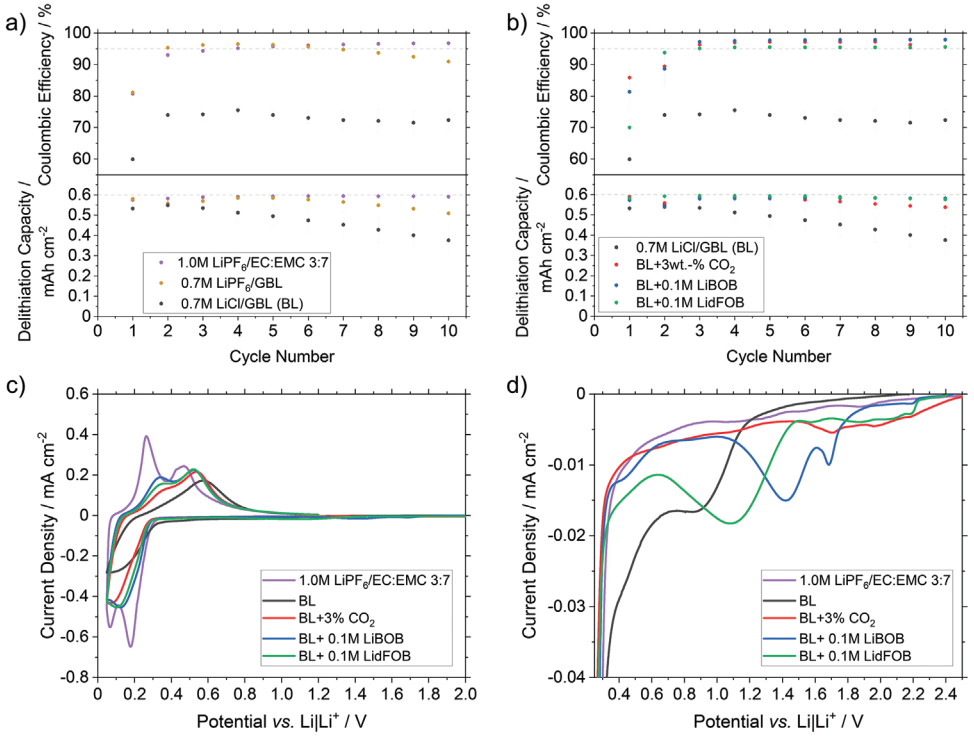

Figure 2. Electrochemical studies of Si||Li metal cells. a,b) Galvanostatic charge/discharge cycling at 0.1 C (0.068 mA cm^{-2}, 358 mA g^{-1}, 1.2–0.05 V vs $Li|Li^+$) of a) 0.7 M LiCl/GBL (BL) compared to the SOTA electrolyte (1 M $LiPF_6$ in EC:EMC 3:7) and 0.7 M $LiPF_6$/GBL, b) comparison of BL electrolyte with electrolyte additives. c,d) Cyclic voltammetry investigation at 50 μV s^{-1} (1.2–0.05 V vs $Li|Li^+$) with several electrolytes. All studies were conducted in a half-cell setup (three-electrode configuration; WE: Si thin film; CE and RE: Li metal; potential control of WE via RE). 0.6 mAh cm^{-2} corresponds to a specific capacity of ≈3200 mAh g^{-1} referred to as pure silicon mass.

For both the BL and SOTA electrolytes, delithiation capacities of 0.58–0.59 mAh cm^{-2}, corresponding to a specific capacity of ≈3200 mAh g_{Si}^{-1} are observed. While a reversible (de-)lithiation with a C_{Eff} of 96% in the fifth cycle is indicated for the SOTA electrolyte, a low C_{Eff} of 74% is achieved with the BL electrolyte stemming from ineffective SEI formation, and thus, irreversible parasitic electrolyte decomposition with ongoing cycles. The BL electrolyte was further compared to an $LiPF_6$ solution in GBL to analyze the impact of the conducting salt on the passivation behavior (Figure 2a). PF_6^- anions are partially reduced during SEI formation and its decomposition products are routinely detected.[9,41] Although not stabilizing with ongoing cycling, the C_{Eff} reaches 96% in the fifth cycle for 0.7 M $LiPF_6$/GBL, which is comparable to the SOTA carbonate electrolyte and shows the notable impact of salt degradation on effective SEI formation. In contrast to insufficient surface passivation of Si with the BL electrolyte, LidFOB, LiBOB, as well as CO_2 (added in form of dry ice) are found to effectively enhance the reversibility of (de-)lithiation in Si‖Li metal cells (Figure 2b) with C_{Eff} values of 97% (CO_2, LiBOB) and 96% (LidFOB) in the fifth cycle. The first cycle C_{Eff} ranges from ≈80% for both boron-based additives to 85% for CO_2. In comparison, the BL electrolyte exhibits a first-cycle C_{Eff} of only ≈60%. For all displayed additives, stable delithiation capacities of ≈0.6 mAh cm^{-2} are observed for ten cycles, which is comparable to the SOTA electrolyte (Figure 2a). EC and FEC were also evaluated as film-forming additives (Figure S1, Supporting Information). For 0.7 M LiCl/EC:GBL 2:8 and 0.7 M LiCl/FEC:GBL 2:8 electrolytes, C_{Eff} values of 92% and 95% in the fifth cycle and first cycle C_{Eff} values of ≈70% are observed, respectively. While passivation with FEC and EC is observed for carbonate solvents, the formed SEI is less effective for the investigated GBL-based electrolyte. This may be related to, for example, lower reduction potentials of EC and FEC compared to GBL or a different reduction mechanism of the carbonate co-solvents due to the presence of GBL leading to a less effective SEI.

Cyclic voltammetry was performed to analyze the reductive decomposition of the electrolytes regarding their SEI formation ability (Figure 2c,d). For all electrolytes, reversible (de-)lithiation of amorphous Li_xSi phases is observed without the formation of the crystalline $Li_{15}Si_4$ phase as indicated by the absence of a sharp oxidation peak at ≈0.4 V versus Li|Li^+.[3,6,7] A lower degree of lithiation shown by lower maximum peak currents for the GBL-based electrolytes and the pure BL in particular, when compared to the SOTA electrolyte may be explained by notably lower ionic conductivities (0.6–1.9 mS cm^{-1}) for the GBL-based electrolytes (**Table 1** and Table S1, Supporting Information).

Table 1. Ionic conductivities of investigated electrolytes determined by impedance spectroscopy (100–1 kHz, 10 mV amplitude).

Electrolyte	Ionic conductivity [mS cm^{-1}]
0.7 M LiCl/GBL (BL)	0.6
BL+3 wt% CO_2	1.0
BL+0.1 M LidFOB	1.9
BL+0.1 M LiBOB	1.8
1 M $LiPF_6$/EC:EMC 3:7	8.5

During the first reductive sweep, a shoulder at ≈0.8 V versus Li|Li^+ is observed prior to Si lithiation for the BL electrolyte (Figure 2d). Regarding the absence of further additives and that LiCl cannot be reduced, this shoulder may be attributed to the reduction of GBL at pure Si. A potentially broad reduction window of GBL and a strong decrease of ethylene gas formation/EC reduction at 0.7–0.3 V versus Li|Li^+ was reported for mixed carbonate/GBL electrolytes on graphite electrodes.[42] For the other electrolytes, the reduction current sharply increases at 0.3 V versus Li|Li^+, which is attributed to Si lithiation. Thus, the increased current flow at 1–0.3 V versus Li|Li^+ for the BL electrolyte may be assigned to irreversible solvent reduction, which is effectively suppressed for GBL-electrolytes containing LiBOB, LidFOB, or CO_2 (Figure 2d). For LidFOB and LiBOB, reduction peaks at 1.5 and 1.2 V versus Li|Li^+ are observed, respectively. According to the literature, these peaks fit the reduction of the additives forming oxalate salts, fluoride in the case of LidFOB, and complex borate/oxalatoborate structures on graphite electrodes.[38,39,43–45] For the BL+3 wt% CO_2 electrolyte, a slightly increased cathodic current is visible from 2–1.2 V versus Li|Li^+ compared to pure BL electrolyte, while notable reduction currents at potentials higher than that of the silicon lithiation are suppressed similarly to the SOTA electrolyte 1 M $LiPF_6$/EC:EMC 3:7 (Figure 2d).

Further, X-ray photoelectron spectroscopy (XPS) was performed for Si electrodes lithiated in the BL and the optimized electrolytes containing additives to investigate the chemical surface composition. Samples were washed with GBL and DMC to remove electrolyte residues.

The apparent elemental surface composition determined by XPS (**Figure 3**a) depicts a higher carbon and a lower Li^+ content for Si electrodes cycled in BL electrolyte compared to the electrolytes containing SEI-forming additives. This hints at a higher amount of organic solvent decomposition products for BL, while an increased fraction of Li-salt products is observed for the additive-containing electrolytes. For F- and B-containing additives, no notable increase in element surface concentration of the respective elements was observed, which can be explained by the low additive concentration, formation of soluble compounds washed off during sample preparation, or evaporation of species in the XPS chamber. Small F-impurities for all samples are related to minor $LiPF_6/PF_5$ contaminations of the XPS measurement chamber. In the C 1s spectra (**Figure 4**b), a pronounced shoulder at ≈286.5 eV is observed for the SEI formed in BL, which can be attributed to C—O and C=O groups.[46–48] Peaks at ≈288 and 290 eV are assigned to alkyl esters containing a $-CO_2R$ functional group, and organic or inorganic carbonate/oxalate compounds, respectively.[46,47,49] Peak deconvolution for those two compound classes reveals an increase in carbonate/oxalate fraction on the electrode surface for electrolytes with additives, while higher alkylester fractions are implied for BL (Figure 4c). Alkylesters or carboxyl compounds may be related to decomposition reactions of GBL, for example, by ring-opening.[50] Although XPS data alone do not provide strict evidence, these observations affirm that solvent decomposition may be dominant for interphase formation in the pure BL electrolyte leading to ineffective passivation and higher cell impedance. The formation of oxalate compounds can be correlated to a more effective SEI formation in

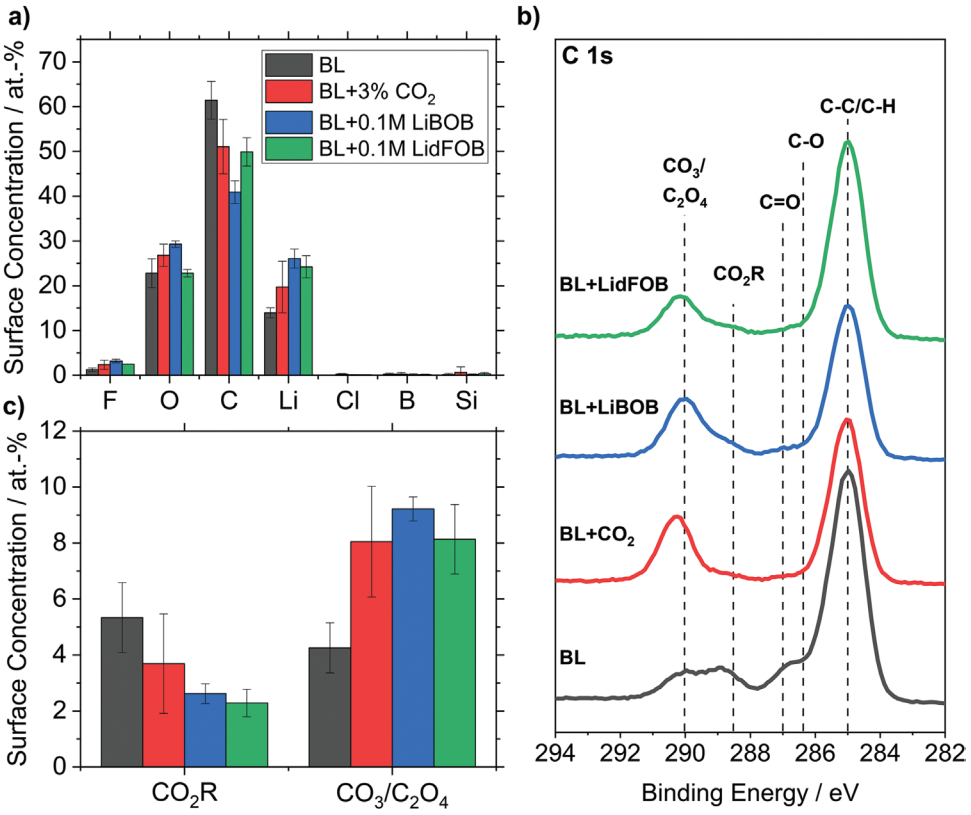

Figure 3. XPS analysis of Si electrodes lithiated to 0.05 V versus Li|Li$^+$ at 0.1 C (within the first charge in Si||Li metal cells) using different GBL-based electrolytes: a) relative elemental surface composition, b) C 1s spectra, c) relative fraction of alkylesters (CO_2R) and organic/inorganic carbonates/oxalates (CO_3/C_2O_4) obtained from fitting of C 1s spectra.

electrolytes based on LiBOB and LidFOB additives.[43,44] For BL+3 wt% CO_2, the peak at 290 eV can be most-likely assigned to lithium carbonate and alkyl carbonates, formed by the reaction of CO_2 with trace amounts of water or alkoxides, as also reported for NCM||graphite LIB full-cells.[51] Single electron reduction of CO_2-forming oxalates or formiate/acetate salts cannot be excluded, either. However, reduction products containing carboxyl groups (≈288–289 eV) are less pronounced in the obtained XPS measurements for BL+3 wt% CO_2.

Sputter depth profiling (SDP) using Ar^+ ion sputtering was performed for BL and BL+3 wt% CO_2 electrolytes to gain insights into the lateral SEI composition. Si 2p, O 1s, and Cl 2p spectra for a Si electrode lithiated in the BL+3 wt% CO_2 electrolyte are displayed in Figure 4.

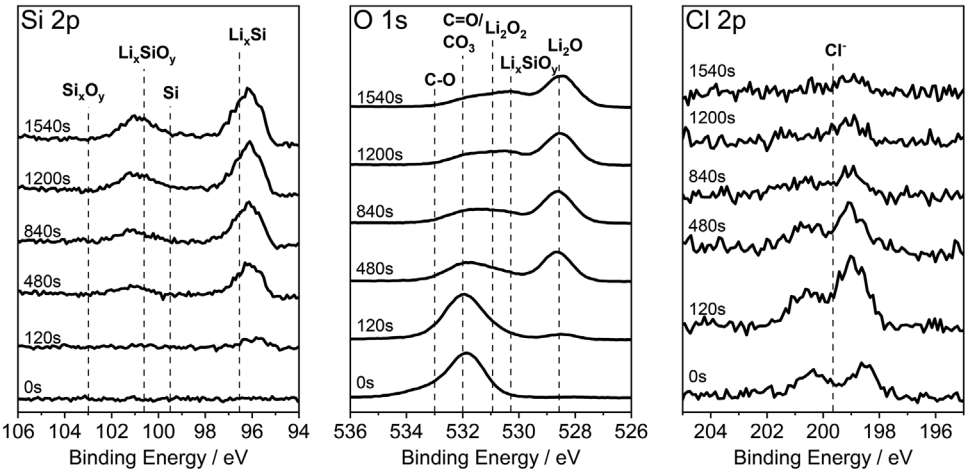

Figure 4. Si 2p, O 1s, and Cl 2p XPS spectra of sputter depth profiling (0.5 kV Ar^+ acceleration voltage) with Si electrodes lithiated to 0.05 V versus Li|Li$^+$ at 0.1 C in BL+3 wt% CO_2 (within the first charge in Si||Li metal cells). Sputter times are indicated next to stacked spectra.

While no Si signal is present for samples lithiated in BL+3 wt% CO_2 without sputtering, two signals start to appear after 120 s and strongly increase after 480 s of sputtering. These signals at 101 and ≈97 eV are attributed to lithium silicates and amorphous lithiated silicon, respectively.[9,52] Peaks in O 1s spectra between 531 and 528 eV are most-likely related to lithium silicates, Li_2O_2 (both 531–530 eV) and Li_2O (≈528.5 eV).[52] Regarding the high Li_2O and Li_xSiO_y/Li_2O_2 content even after continuous sputtering, it is likely that these compounds are formed during Ar^+ sputtering by the reaction of Li_xSi with O-containing species. Sample degradation due to high-energy Ar^+ sputtering has been analyzed in several studies.[53] Small amounts of chloride (≤0.5 at%) have been found after 480 s of sputtering, which indicates that only minor amounts of conducting salt from pre-lithiation are incorporated within the SEI for BL+3 wt% CO_2. In contrast, Si peaks start to appear after 480 s of sputtering on samples lithiated in pure BL (Figure S2, Supporting Information), which qualitatively implies a thicker overlayer on Si. A similar lateral layer composition as for BL+3 wt% CO_2 is displayed in O 1s spectra for pure BL after longer sputtering times affirming that a thicker layer of organic/inorganic decomposition products is present.

In summary, electrochemical and spectroscopic analysis show that an effective, electronically passivating interphase is formed on Si thin films using GBL-based electrolytes optimized with additives (LidFOB, LiBOB, CO_2). The results imply reduced solvent reduction and a thinner SEI for the optimized electrolytes compared to the pure LiCl/GBL electrolyte. Only minor incorporation of Cl^- into the SEI at Si was found. These properties can be considered as suitable for the practical application of the electrolytes for electrolytic pre-lithiation of silicon-based anodes.

2.2. Application of Optimized Electrolytes for Electrolytic Pre-Lithiation

Lithiation experiments were conducted in glassy carbon (GCa)||Si pouch cells (three-electrode configuration) to investigate the viability of electrolytic pre-lithiation with the optimized GBL-based electrolytes. GCa was chosen as the CE for electrolytic pre-lithiation due to its high mechanical and chemical stability, as well as sufficient activity toward chloride oxidation. Si (WE) and GCa (CE) potential profiles for lithiation of Si via electrolysis using the BL+3 wt% CO_2 electrolyte are depicted in **Figure 5**a.

A sloping profile typical for the formation of amorphous Li_xSi is observed for Si electrodes.[54] Compared to the electrochemical lithiation of Si in the SOTA electrolyte 1 M $LiPF_6$/EC:EMC 3:7 (cf. Figure S3, Supporting Information), the plateau is slightly shifted to lower values by ≈60 mV and exhibits less slope. This potential shift may be attributed to increased overpotentials during lithiation caused by different ionic conductivities of the electrolytes (see Table 1). Further, a small change in the Li|Li^+ redox potential due to the different solvents and Li^+ activity may contribute to that. For the GCa electrode, a flat plateau at 3.9 V versus Li|Li^+ is displayed, which is attributed to the continuous formation of elemental gaseous chlorine. The potential profiles for electrolytic pre-lithiation using the other electrolytes are depicted in the Supporting Information including BL (Figure S4a, Supporting Information), BL+0.1 M LiBOB (Figure S4b, Supporting Information), and BL+0.1 M LidFOB (Figure S4c, Supporting Information). Si electrodes lithiated via electrolysis were de-lithiated in Si||Li metal cells to analyze the C_{Eff} of electrolytic pre-lithiation (Figure 5b). While a higher DoP can be achieved by decreasing the lithiation cut-off potential, only low absolute delithiation capacities of up to ≈0.3 mAh cm^{-2} are observed for the different additive-containing electrolytes. The maximum delithiation capacity corresponds to a C_{Eff} of 35–40% for pre-lithiation. The low C_{Eff} during pre-lithiation is ascribed to the partial dissolution of elemental chlorine in the electrolyte, which causes self-discharge, as discussed in the following section. For BL+3 wt% CO_2, slightly higher delithiation capacities could be extracted than for the electrolytes optimized with the borate salts. Reasons for this may be differences in SEI formation resulting in, for example, reduced permeability for Cl_2, which may decrease self-discharge. Further reasons may be a reduced solubility of Cl_2 in BL+3 wt% CO_2 caused by the presence of dissolved CO_2. Similar electrochemical results were

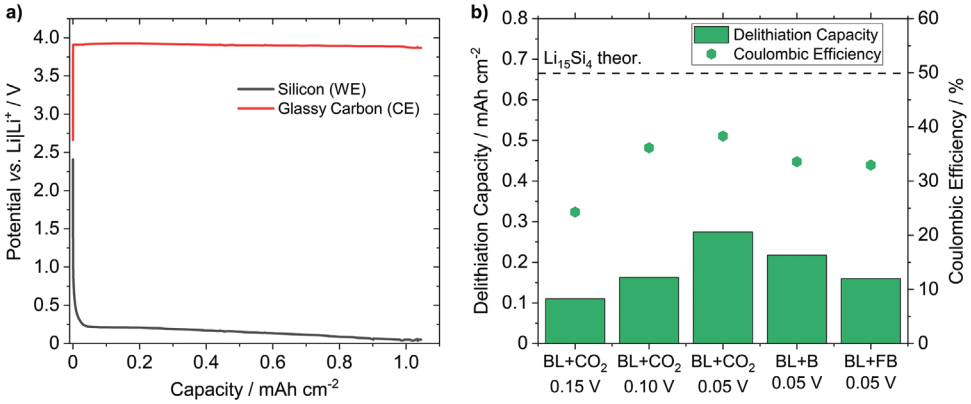

Figure 5. a) Potential profiles from galvanostatic pre-lithiation (0.1 C, 358 mA g^{-1}) of Si electrodes using salt electrolysis (electrolyte: BL+3 wt% CO_2). Lithiation was performed until the Si cut-off limit of 0.05 V versus Li|Li^+ was reached. Cell setup: GCa||Si pouch cell, half-cell setup, three-electrode configuration, WE: Si, CE: GCa, RE: Li metal. b) Galvanostatic delithiation capacities of pre-lithiated Si electrodes in Si||Li metal pouch cells (0.1 C, 358 mA g^{-1}, upper cut-off potential: 1.2 V vs Li|Li^+; half-cell setup; three-electrode configuration; WE: Si, CE, and RE: Li metal). Prior to delithiation, electrolytic lithiation was performed in GCa||Si pouch cells using varying electrolytes and cut-off potentials versus Li|Li^+ displayed on the *x*-axis inscription: i) BL+CO_2: BL+3 wt%CO_2; ii) BL+B: BL+0.1 M LiBOB; iii) BL+FB: BL+0.1 M LidFOB.

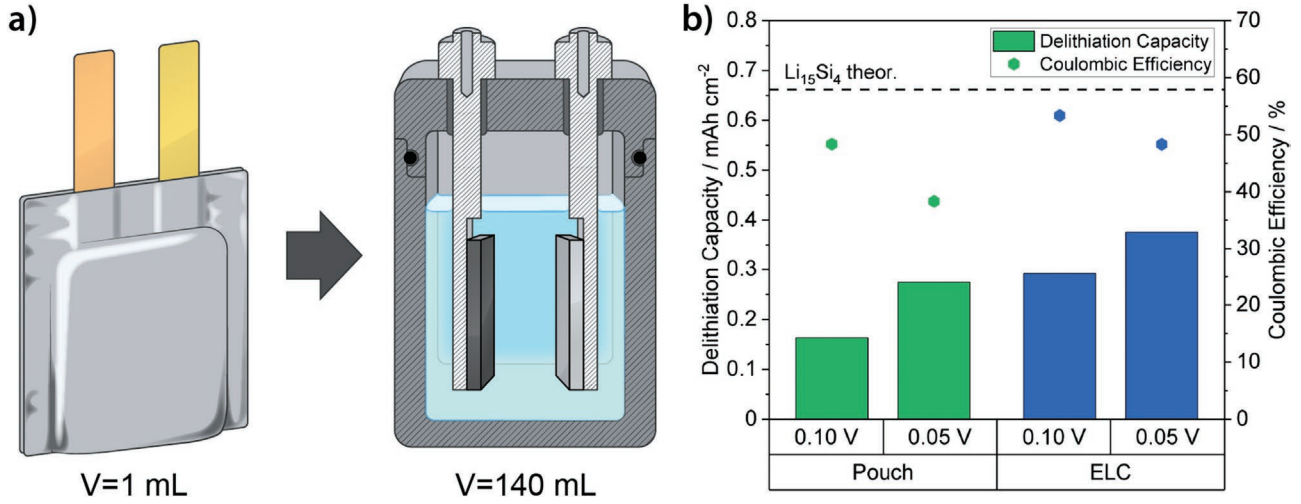

Figure 6. a) Schematic comparison of pouch cell and electrolysis cell (ELC). b) Galvanostatic delithiation of pre-lithiated Si electrodes in Si||Li metal pouch cells (0.1 C, 358 mA g^{-1}, upper cut-off potential: 1.2 V vs Li|Li^+; three-electrode configuration; WE: Si (pre-lithiated); CE and RE: Li metal). Prior to delithiation, electrolytic pre-lithiation was performed in GCa||Si pouch cells (left, green) and the electrolysis cell (ELC, right, blue) using BL+3 wt% CO_2 at varying cut-off potentials versus Li|Li^+ displayed on the *x*-axis inscription.

obtained using an in-house built electrolysis cell (ELC) with a higher distance of 2 cm between WE and CE (**Figure 6**a, for further details, cf. Figure S5, Supporting Information). For the BL+3 wt% CO_2 electrolyte, higher delithiation capacities and a C_{Eff} of ≈50% were found, which is attributed to a significantly higher dilution of Cl_2 and a largely increased distance between WE and CE in the ELC lowering diffusional mass transport of Cl_2 to the WE. This leads to reduced parasitic self-discharge reactions at the Si electrode (Figure 6b) and shows the potential for large-scale application with an optimized electrolysis setup.

2.3. Chlorine/Chloride Shuttle Mechanism for Electrolytic Pre-Lithiation

In the following, the solubility of gaseous chlorine in the electrolyte was analyzed to investigate the origin of these notable parasitic side reactions. Therefore, 2 wt% of VC was added post-mortem to a sample of BL+3 wt% CO_2 electrolyte extracted from a pre-lithiation pouch cell after electrolysis to detect the formation and dissolution of chlorine in the electrolyte. The presence of Cl_2 could be shown by the detection of the addition product of Cl_2 to the C=C double bond of VC via solid-phase micro extraction-gas chromatography-mass spectrometry (SPME-GC-MS) (**Figure 7**a,b). Dissolution of a similar electrolyte sample extracted from pre-lithiation pouch cells in 0.5 M LiBr/acetonitrile and subsequent extraction with cyclohexane showed oxidation of Br^- to elemental bromine, which also confirms the dissolution of Cl_2 in the electrolyte (Figure 7c).

It becomes obvious, that a notable amount of chlorine does not evaporate, but is dissolved in the electrolyte for the used cell setups. Thereby, it can diffuse to the Si WE leading to a self-discharge shuttle mechanism and reduction of Cl_2 to Cl^- anions at the Si surface. This may be facilitated by incomplete

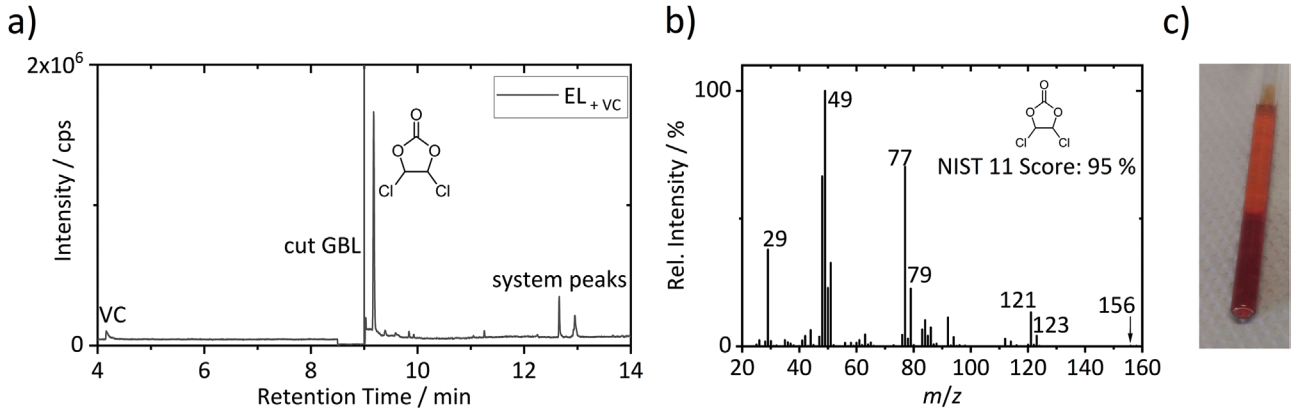

Figure 7. a) SPME-GC-MS chromatogram of 0.7 M LiCl/GBL +3 wt% CO_2 +10 wt% VC after electrolysis and b) the corresponding MS spectrum for observed dichloroethylene carbonate. Electrolysis was performed in GCa||Si pouch cells (0.1 C, 358 mA g^{-1}, half-cell setup; three-electrode configuration; WE: Si, CE: GCa, RE: Li metal, lithiation until al Si-WE potential of 0.05 V vs Li|Li^+ was reached). For the detection of Cl_2, VC was added after pre-lithiation to the electrolyte sample. The main GBL peak at ≈8.7 min was cut off to impede the overload of the detector. c) 0.7 M LiCl/GBL +3 wt% CO_2 after electrolysis dissolved in 0.5 M LiBr/acetonitrile and extraction of formed Br_2 with cyclohexane (upper phase).

electronic passivation of the SEI or the formation of a pristine Si surface caused by volume expansion during lithiation. Contact element formation between Cu and Li_xSi may enable corrosion due to electronic contact between Cu and Li_xSi even if the Si surface is effectively passivated, and accelerates corrosion due to Cl_2. However, no notable formation of solvent decomposition products could be observed by means of SPME-GC-MS after electrolytic pre-lithiation with BL+3 wt% CO_2 (Figure S6, Supporting Information). This implies that the solvent is not notably affected by the presence of the oxidative species.

Apart from that, the dissolution of current collector metals into the electrolyte due to corrosion with Cl_2 was confirmed by inductively coupled plasma-optical emission spectroscopy (ICP-OES) (**Table 2**).

A notable amount of current collector metals Cu, Ni (from the Si WE), and Al (from the GCa CE) are dissolved upon electrolysis. The ICP-OES data support the proposed shuttle mechanism of Cl_2/Cl^- species, as the Cu and Ni concentrations (801 and 53 ppm, respectively) are notably increased for the electrolytes from the electrolysis approach compared to the electrolyte from electrochemical lithiation, that is, without oxidation of Cl^- (100 and 0 ppm, Table 2). Cu and Ni are used as WE current collector and electrical contact and are not exposed to oxidative potentials. This shows that diffusion of Cl_2 to the WE and electrochemical corrosion of these metals takes place (refer to **Figure 8**). A low concentration of Cu cations for the electrolyte not exposed to oxidative conditions may be explained by a native oxide layer on copper foil, which may be partially dissolved in the investigated chloride-containing electrolytes.[55] The effect is potentially enhanced by the high surface area of dendritic copper foil.

Despite these parasitic self-discharge reactions lowering pre-lithiation capacity and Coulombic efficiency, the electrolytic pre-lithiation of Si electrodes could be successfully performed.

Aiming at insights into electrode kinetics, which are related to the SEI properties formed in the GBL-based electrolytes and potential degradation caused by electrolysis, pre-lithiated Si electrodes were analyzed by electrochemical impedance spectroscopy (EIS). To exclude the impact of a counter electrode on the measured impedance, 12 mm disks were punched out from 3 × 3 cm Si electrodes, which were pre-lithiated by electrolysis to 0.05 V versus $Li|Li^+$. The electrodes were washed to remove residues of the pre-lithiation electrolyte and reassembled into symmetrical Si||Si coin cells using 1 M $LiPF_6$/EC:EMC 3:7 as SOTA electrolyte. Impedance spectra are depicted in **Figure 9**.

Table 2. Concentration of metal ions originating from current collectors in a BL+3 wt%CO_2 electrolyte sample extracted from Si||Li metal pouch cells (half-cell setup; three-electrode configuration; WE: Si, CE, and RE: Li metal) after electrochemical lithiation (PreLi vs. Li), or GCa||Si pouch cells (half-cell setup; three-electrode configuration; WE: Si, CE: GCa, RE: Li metal) after electrolysis (PreLi vs GCa).

	PreLi versus Li	PreLi versus GCa
c(Cu)/mg kg^{-1}	100 ± 2	801 ± 25
c(Al)/mg kg^{-1}	<LOQ	74 ± 4
c(Ni)/mg kg^{-1}	<LOQ	53 ± 3

For both setups, pre-lithiation was conducted at 0.1 C, 358 mA g^{-1}, until a Si-WE potential of 0.05 V versus $Li|Li^+$ was reached. Concentrations were determined by ICP-OES.

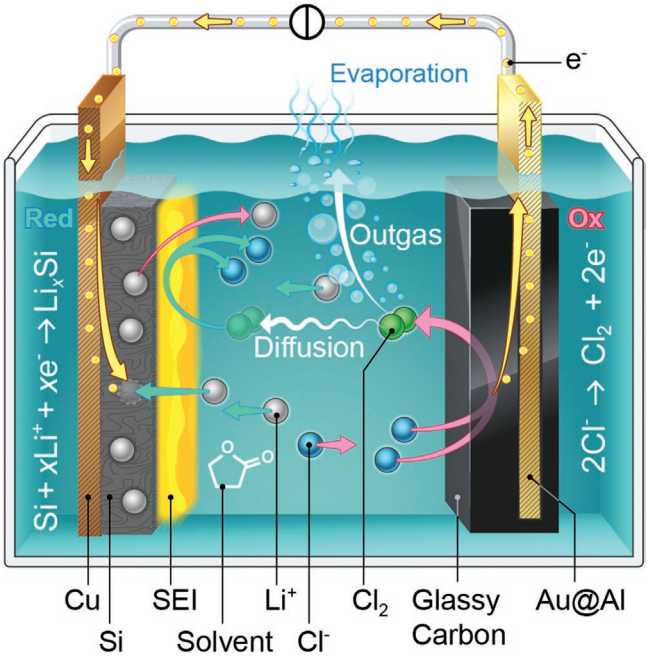

Figure 8. Schematic illustration of the Cl_2/Cl^- shuttle mechanism in an electrolysis bath used for electrolytic pre-lithiation. The electrolyte is based on GBL and LiCl as salt. During electrolysis, the Si negative electrode is pre-lithiated, while Cl^- oxidation to form gaseous Cl_2 takes place at the glassy carbon positive electrode. Cl_2 can be dissolved in the electrolyte and shuttle to the negative electrode, where it can be reduced to Cl^-. As a result, Cl^- formation will lead to self-discharge of the negative electrode.

For all spectra, a depressed semicircle is displayed in the high-frequency region above 1–10 Hz. The radius of this semicircle is approximately an order of magnitude larger for Si||Si cells consisting of pristine Si electrodes far from lithiation potential, thus, representing Li^+ blocking conditions (Figure S7, Supporting Information). Thus, this semicircle may be attributed to Li^+ charge transfer (including interphase) processes.[56] Herein, its radius is used as an approximate qualitative measure for the charge transfer and interphase resistance. The ≈30° slope followed by a 70°–80° linear region in the low-frequency region below 10–1 Hz is related to diffusive transport processes and may reflect restricted diffusion behavior.[57] Compared to Si electrodes electrochemically lithiated in the SOTA carbonate electrolyte, Si electrodes electrolytically pre-lithiated in the BL electrolyte exhibit a larger convoluted semicircle in the region above 10 Hz (Figure 9). On the one hand, this may be linked to a higher charge transfer/interfacial resistance, which is related to a thicker or less Li^+-conducting SEI caused by excessive solvent reduction (see Figures 2 and 3). On the other hand, the larger charge transfer/interfacial semicircle is also related to the state-of-charge (SOC) of the electrode[58] revealing nearly blocking conditions and a low lithium content of Si for pre-lithiation with the BL electrolyte. For LiBOB- and LidFOB-containing additives, charge transfer kinetics of pre-lithiated Si thin films are comparable to Si electrodes electrochemically lithiated in 1 M $LiPF_6$/EC:EMC 3:7. In contrast to that, the charge transfer/interphase resistance for the samples from electrolytic pre-lithiation in BL+3 wt% CO_2 may be even lower than that of the SOTA carbonate electrolyte system.

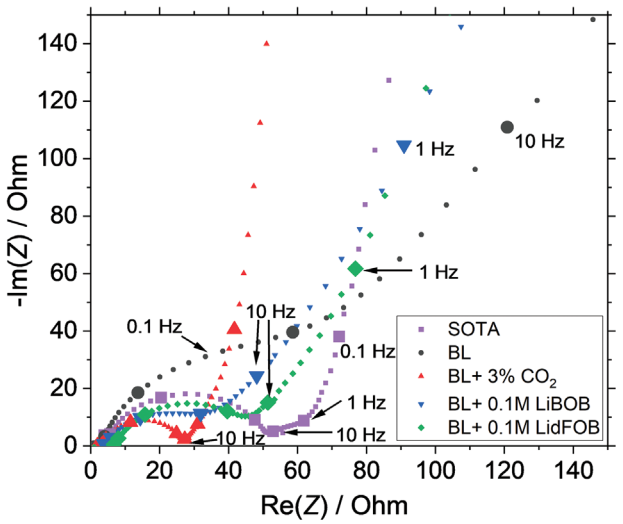

Figure 9. EIS spectra for symmetrical Si||Si cells (coin cells; two-electrode configuration; 100kHz–100mHz, 10 mV amplitude) using 1 M $LiPF_6$/EC:EMC 3:7 (SOTA) as electrolyte. Prior to cell assembly, Si electrodes were pre-lithiated in Si||GCa pouch cells (half-cell setup; three-electrode configuration; WE: Si; CE:GCa, and RE: Li metal) to 0.05 V versus $Li|Li^+$ using the electrolytes depicted in the figure caption. Electrodes pre-lithiated using the SOTA electrolyte (purple) were extracted from S||Li pouch cells (half-cell setup; three-electrode configuration; WE: Si; CE and RE: Li metal), pre-lithiation to 0.05 V versus $Li|Li^+$. Frequency decades are additionally marked by enlarged data points.

However, only a qualitative comparison of charge transfer kinetics is valid due to potential differences in SOC of the electrolytically pre-lithiated electrodes and the electrodes lithiated in the SOTA electrolyte (see Figure 5b). In summary, the impedance spectra show that Li^+-permeable interlayers are formed using the GBL electrolytes optimized with additives, and no notable degradation of electrode kinetics is implied.

Furthermore, SEM analyses were performed to investigate whether the contact of lithiated Si electrodes with Cl_2 leads to morphology degradation (**Figure 10**a–c). A comparison between pristine Si electrodes, Si lithiated in Si||Li metal cells using the SOTA electrolyte (in 1 M $LiPF_6$/EC:EMC 3:7), and Si lithiated via electrolysis in GCa||Si cells with BL+3 wt% CO_2 did not reveal any structural degradation due to the electrolysis setup and alternative electrolyte formulation. In general, sputter-deposited Si was found to form particles of ≈100–800 nm size at Cu dendrites in the pristine state (see Figure S8, Supporting Information). Particle swelling and slight cracking were most dominant for the SOTA electrolyte, which can probably be connected to the highest degree of lithiation considering self-discharge and lower delithiation capacity for the electrolytically lithiated Si sample. The size and crack structure of Si particles imply that outer particles relative to the current collector surface are lithiated preferred compared to particles close to the Cu surface. This might be linked to increased particle/electrolyte interface area for outer, more exposed particles compared to the inner ones, and stronger Li^+ depletion closer to the current collector.

In addition to that, no significant change of surface composition could be found in XPS spectra by comparison of electrochemically lithiated Si electrodes and Si electrodes lithiated via electrolysis both using the BL+3 wt% CO_2 electrolyte (Figure S9, Supporting Information). The sputter depth profile for Si 2p indicates a similar overlayer thickness for lithiation via electrolysis compared to lithiation using Li metal as CE (cf. also Figure 4). Notable amounts of chlorinated solvent decomposition products could be neither detected on the Si surface via XPS, nor in cycled BL+3 wt% CO_2 electrolyte samples without VC via SPME-GC-MS. Thus, it is concluded that at least small concentrations of chlorine do not notably affect the electrode morphology and SEI composition.

2.4. Analysis of Pre-Lithiated Si Electrodes in NCM111||Si Full-Cells

NCM111||Si full-cells were assembled with Si electrodes pre-lithiated via electrolysis to validate the practicality of the electrolytic pre-lithiation method as a proof-of-concept. The nominal N/P capacity balancing was experimentally adapted to the DoP to impede the plating of Li metal at the Si/electrolyte interface. Thus, an approximately constant N capacity excess, corresponding to a constant safety factor,[34] is maintained. The DoP is defined according to literature as pre-lithiated capacity relative to the Si nominal first charge/lithiation capacity (≈4000 mAh g^{-1}).[34] Therefore, the low pre-lithiation C_{Eff} as discussed above leads to a low actual SOC of the Si electrode even though a high pre-lithiation dosage, that is, a high DoP is applied. As a consequence, high DoPs of 50% were applied to achieve a substantial lithium reservoir in the Si electrodes. Specific discharge capacities and C_{eff} values for pre-lithiated NCM111||Si full-cells are displayed in **Figure 11**a.

All cells exhibit an initial specific discharge capacity of ≈140–150 mAh g^{-1}, which is based on the cathode capacity. While the reference cells without pre-lithiation and the cells pre-lithiated with the pure BL electrolyte achieve a C_{Eff} of 88.5% and 87.4% in the first cycle, respectively, a C_{Eff} of 89–90% is observed for

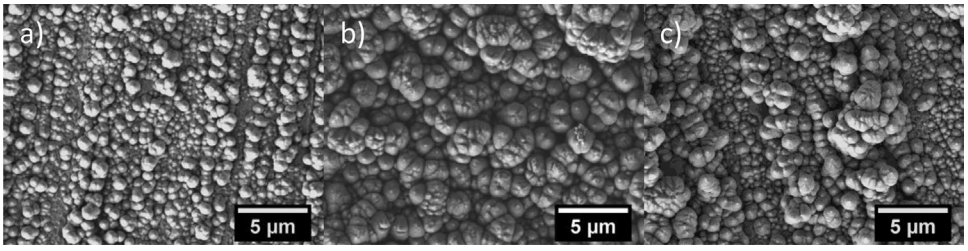

Figure 10. SEM images of a) a pristine Si thin film electrode, and lithiated Si electrodes in b) Si||Li metal pouch cells (1 M $LiPF_6$/EC:EMC 3:7) and c) GCa||Si pouch cells (BL+3 wt% CO_2). Samples were lithiated to a cut-off potential of 0.05 V versus $Li|Li^+$ at 0.1C for (b,c).

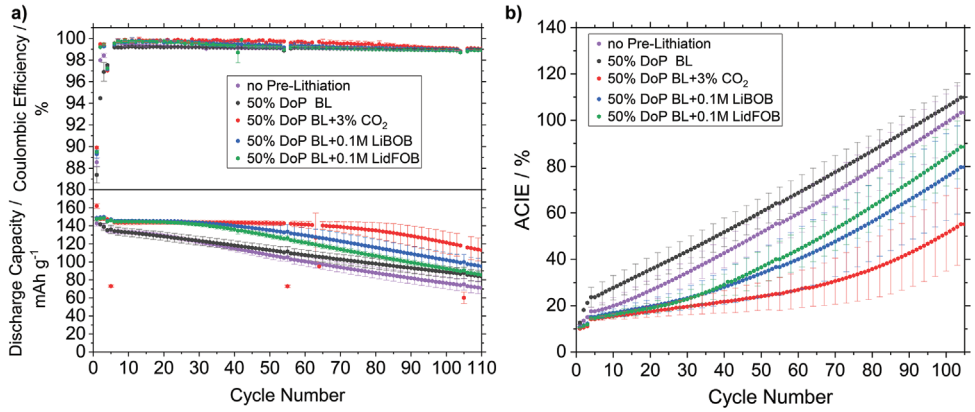

Figure 11. Galvanostatic charge/discharge cycling of NCM111||Si cells (0.5 C CCCV, 4.2–2.5 V, full-cell setup, two-electrode configuration, 1 M $LiPF_6$/EC:EMC 3:7+10 wt% FEC) using pre-lithiated Si electrodes with the electrolytes mentioned in the figure legend. Electrolytic pre-lithiation was conducted in Si||GCa pouch half-cells, three-electrode setup (WE: Si, CE: GCa, RE: Li metal) until a charge corresponding to 50% DoP = 2000 mAh g^{-1} (Si) was reached. Three formation cycles were performed at 0.1 C CCCV. After formation and each 50th cycle, a characterization cycle with a subsequent pulse test was conducted. a) Specific discharge capacities and C_{Eff} values, b) accumulated Coulombic inefficiency (ACIE) plotted versus cycle number. The degree of pre-lithiation (DoP) is here defined as a 50% lithiation charge relative to the Si nominal first lithiation capacity (≈4000 mAh g^{-1}).

cells pre-lithiated with the optimized electrolytes. The discharge capacities of non-pre-lithiated reference cells and cells pre-lithiated in BL continuously drop with ongoing cycling, which is a result of ongoing active lithium losses due to SEI (re-)formation (135–138 mAh g^{-1} after three formation cycles). Apart from that, pre-lithiation with BL+0.1 M LiBOB/LidFOB leads to stable discharge capacities of ≈145 mAh g^{-1} at 0.5C for ≈30 cycles. For pre-lithiation using BL+3 wt% CO_2, ≈145 mAh g^{-1} is observed for ≈70 cycles. In this region with high capacity retention, the C_{Eff} for optimized pre-lithiation (99.6–99.7% in the 20th cycle) is substantially higher than that for the reference cells (99.1–99.2%, 20th cycle), which explains the improved capacity retention. In the following cycles, continuous capacity fading comparable to those of the reference cells sets in with significantly lower C_{Eff} of 99.1% in the 80th cycle.

The successive capacity loss for reference and BL pre-lithiated cells is essentially caused by the trapping of active lithium at the Si electrode due to reductive side reactions as continuous SEI formation is enhanced, for example, by the large volume changes and cracking.[6,7,15,18] By pre-lithiation, this "trapping" or loss is compensated by the formation of a lithium reservoir present in the described cycle range with high capacity retention. The electrochemical performance of cells pre-lithiated with BL electrolyte implies that no substantial compensation of Li loss was achieved due to the lacking passivation behavior of the SEI on Si, as stated before. With respect to standard deviation, no significant deterioration of the Si performance is observed compared to the reference cells, though. For cells pre-lithiated with BL+3 wt% CO_2, an overall capacity retention of 78% is observed in the 100th cycle while reference cells without pre-lithiation achieve only 54%. The increased capacity retention for pre-lithiation with BL+3 wt% CO_2 compared to 0.1 M LidFOB/LiBOB in GBL (62/68% in the 100th cycle) may be explained by a higher effective degree of pre-lithiation for BL+3 wt% CO_2 as implied in Figure 6b. The formation of a lithium reservoir is further depicted by a reduced slope of the accumulated Coulombic inefficiency (ACIE) for pre-lithiated cells compared to the ones without pre-lithiation (Figure 11b). When the reservoir is consumed, the capacity fading of pre-lithiated cells becomes comparable to those of the reference cells. In addition to that, the area-specific impedance (ASI) measured after formation and every 50 cycles is in the same range for pre-lithiated and reference cells proving that the pre-lithiation process does not deteriorate the cell performance (Figure S10, Supporting Information). As the loss of active lithium is more pronounced for pure Si thin films (=100% Si) compared to practical Si/C composites (Si content typically below 20%), the consumption of the reservoir is also clearly revealed by a drop in C_{Eff} and an increase in the slope of ACIE for pre-lithiated cells (Figure 11b). Active lithium loss is further depicted in potential profiles of NCM111||Si cells, which were evaluated in a three-electrode full-cell setup (**Figure 12**).

For cells without pre-lithiation, the end-of-charge (EOC) and end-of-discharge (EOD) potentials of the Si potential profile continuously shift to higher values after formation (Figure 12a). The EOD potential of Si after formation (0.9–1 V vs $Li|Li^+$) indicates polarization and complete delithiation of Li_xSi. During the presence of a Li reservoir in the first 50 cycles, the Si potential curve for the pre-lithiated cell exhibits an EOD potential of 0.6–0.8 V versus $Li|Li^+$, which shows that Si is not completely delithiated (Figure 12b). With consumption of the reservoir, the EOC and EOD potentials of Si rise, thus, leading to the increasing polarization of Si in the delithiated state after 60–70 cycles. In addition to that, this distinctive Si potential shift leads to an increase of the NCM (P) potential window leading to incomplete lithiation of P during discharge (EOD potential) and a higher degree of delithiation during charge (EOC potential), which may lead to accelerated degradation of P. In conclusion, a significant performance gain for NCM111||Si full-cells could be demonstrated due to the compensation of active lithium losses by electrolytic pre-lithiation.

Although suffering from a low C_{Eff} due to cross-talk phenomena in lab-scale cells, practical application of the electrolytic pre-lithiation method could be successfully demonstrated. No severe impact of strongly oxidizing electrolysis byproducts, such as Cl_2 on the performance of the Si active material,

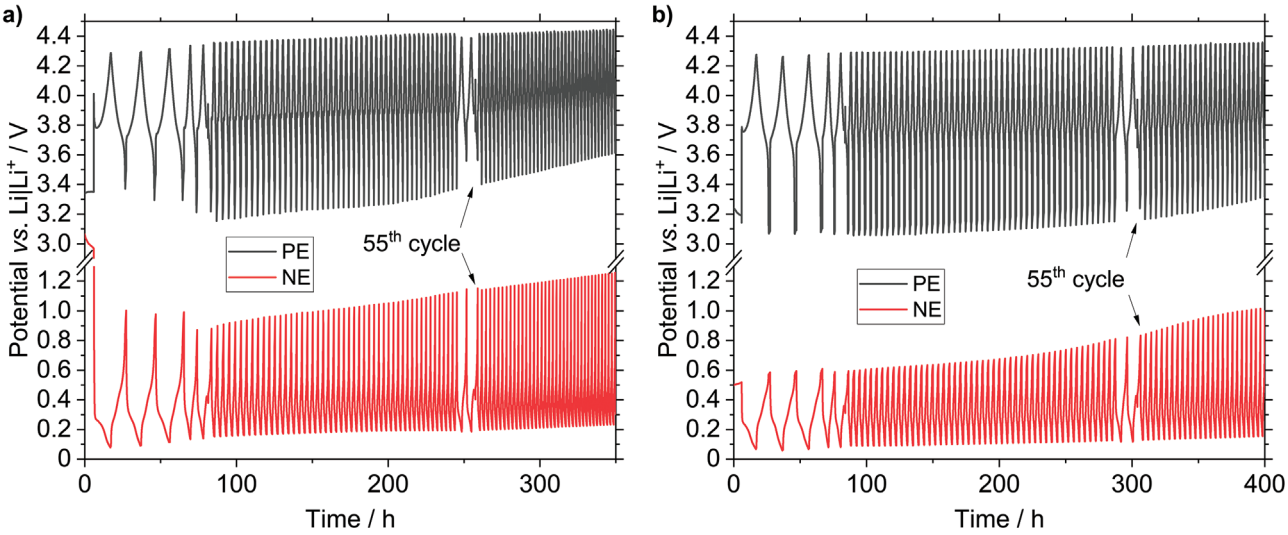

Figure 12. Potential profiles for P (NCM111) and N (Si) recorded during galvanostatic cycling of NCM111||Si pouch cells (0.5 C CCCV, 4.2–2.5 V, full-cell setup, three-electrode configuration; electrolyte: 1 M $LiPF_6$/EC:EMC 3:7+10 wt% FEC). a) Reference cell without pre-lithiation, b) the Si electrode was pre-lithiated via electrolysis to 50% lithiation capacity relative to the Si nominal lithiation capacity in the BL+3 wt% CO_2 electrolyte.

in particular with optimized electrolyte formulations, could be observed. Nevertheless, contact of Cl_2 to the negative electrode causing current collector dissolution may lead to performance loss and difficulties for technical application of the pre-lithiation process on a larger scale and should be impeded by, for example, the removal of dissolved Cl_2.

3. Conclusion

Pre-lithiation via an electrolysis approach using lithium chloride (LiCl) was investigated and successfully demonstrated for Si thin films as a model electrode. Due to the use of LiCl as cost-efficient electrolysis salt, GBL was chosen as the solvent providing the highest LiCl solubility and highest ionic conductivity of all electrolyte solvent candidates. A low Coulombic efficiency (C_{Eff}) for the pure BL electrolyte (0.7 M LiCl in GBL) in Si||Li metal cells could be attributed to inferior passivation/SEI formation characteristics of pure GBL. The solvent reduction could be significantly minimized by the additives LiBOB, LidFOB, and CO_2, as indicated by cyclic voltammetry studies. The C_{Eff} could be improved from 75% for BL to 95–96% for the optimized additive-containing electrolytes in Si||Li metal cells, which is in the range of SOTA commercial carbonate electrolytes (here: 1 M $LiPF_6$/EC:EMC 3:7). An increased fraction of carbonate/oxalate compounds on the surface, as well as a thinner layer of reductive decomposition products, was observed by XPS, and could be correlated to effective passivation behavior for the additive-containing electrolytes compared to the pure GBL-based electrolyte. Only small residual fractions of Cl^- were found within the SEI, which may be beneficial for the performance of typical NCM-based positive electrode materials.

Electrolytic pre-lithiation of Si model electrodes was investigated in GCa||Si pouch cells. Thereby, the formation of Cl_2 was evidenced by an oxidation plateau at ≈3.9 V versus $Li|Li^+$, and in the electrolyte via indirect detection with VC and subsequent formation of dichloroethylene carbonate using SPME-GC-MS. It was further observed that Cl_2 partially dissolves in the electrolyte leading to corrosion of the WE current collector (dissolution of Cu and Ni species). Only a low pre-lithiation C_{Eff} of ≈35% was found in lab-scale GCa||Si pouch cells. A higher C_{Eff} of ≈50% could be observed for a beaker ELC with a higher electrode distance and a large electrolyte volume leading to increased dilution of oxidative chlorine. EIS, SEM, and XPS measurements did not indicate morphological or SEI degradation, although Si electrodes were exposed to Cl_2. Electrolytic pre-lithiation could be successfully demonstrated in NCM111||Si full-cells. Compared to not pre-lithiated reference cells, an initial capacity increase from ≈135 to ≈145 mAh g^{-1} for pre-lithiated cells was observed after formation cycles. The capacity retention in the 100th cycle could be significantly increased from 54% to 78%.

Although the C_{Eff} of electrolytic pre-lithiation in lab-scale cells must be improved to ensure precise control of the pre-lithiation degree, in particular for higher practical mass loadings, the potential for large-scale application could be successfully shown. A Cl_2/Cl^- shuttle mechanism was proposed, which is initiated by the diffusion of Cl_2 to the pre-lithiated electrode and is considered as a major reason for parasitic side reactions and self-discharge of pre-lithiated Si. The shuttle mechanism might be minimized using flow cells purging Cl_2-containing electrolytes from the cell compartment and removal of Cl_2 by purifying or degassing the electrolyte. Thus, the major drawbacks pointed out can be considered as technical challenges, which can be resolved using an appropriate, optimized electrolysis setup. Different organic anions, for example, lithium oxalate or acetate forming less corrosive and toxic oxidation products as CO_2 may be a convenient alternative to LiCl, while their application is hampered by solubility issues in organic solvents and/or low cathodic stability. In the future, the electrolysis method should be transferred to the pre-lithiation of graphite and

Si/graphite composite electrodes for a practically viable compromise between high energy and lifetime.

4. Experimental Section

Materials, Electrodes, and Electrolyte Components: Silicon thin films on dendritic copper foil (Schlenk AG) were prepared using an RF-magnetron sputter device (BesTec-Berlin GmbH, target: *n*-type monocrystalline silicon purity 99.99%, FST Freiberger Silicium und Targetbearbeitung GmbH) with a base pressure of $<10^{-7}$ mbar. 3 × 3 cm copper substrates (electrolytic copper foil, Sc) were sputter-coated using RF sputtering at 90 W power, 5×10^{-3} mbar pressure (Ar atmosphere), and the distance between the target and substrate was set to 7 cm. Si thin film negative electrodes were dried at 80 °C under reduced pressure ($<10^{-2}$ mbar) for 2 h before use. $LiNi_{1/3}Co_{1/3}Mn_{1/3}O_2$ (NCM111) positive electrodes (CUSTOMCELLS Holding GmbH) with an active material content of 90% (4.1 ± 0.1 mg cm^{-2}) were dried at 110 °C for at least 12 h under reduced pressure ($<10^{-2}$ mbar) and subsequently used without further preparation. The pre-lithiation electrolyte salt lithium chloride (LiCl; Sigma Aldrich, purity: 99.98% trace metals basis) was dried at 150 °C under reduced pressure ($<10^{-2}$ mbar) for 12 h before use. The major pre-lithiation electrolyte solvent GBL (Sigma Aldrich, purity: 99%) was dried statically over molecular sieves (Sigma Aldrich, 0.3 nm) for 24 h and subsequently dynamically dried via a column filled with molecular sieves resulting in a water content below 15 ppm measured by Karl–Fischer titration. LidFOB (abcr GmbH, purity: 99%), LiBOB (abcr GmbH, purity: 97%), lithium hexafluorophosphate ($LiPF_6$), ethylene carbonate (EC) and VC (both Targray, purity: 99.9%), FEC (BASF, 99.9%), lithium bromide (LiBr, Sigma Aldrich, purity: 99.99% trace metals basis), and a mixture of EC:EMC (3:7 by wt.; E-Lyte Innovations GmbH, purity: 99.9%, H_2O content below 20 ppm) were used as received. CO_2 added in form of dry ice (Westfalen AG) was used as an additive for GBL-based electrolytes. Due to trace amounts of water, the water content of 0.7 M LiCl/GBL+3 wt% CO_2 was ≈30 ppm as determined by Karl Fisher titration. Cyclohexane and acetonitrile (both Fisher Scientific, purity: HPLC grade) for detection of Cl_2 were purified and dried via a solvent purification system.

Cell Preparation and Electrochemical Measurements: All constant-current (CC) experiments were performed at 20 °C using Maccor 4000 battery testers (Maccor Inc.) For characterization of the electrolytes, galvanostatic charge/discharge cycling (1.2–0.05 V vs Li|Li^+, 0.068 mA cm^{-2}, 358 mA g^{-1}, 0.1C) was performed in Si||Li metal Swagelok T-cells (half-cell setup, three-electrode configuration; WE potential control via the RE).[59] Each half cycle was followed by a constant-potential (CP) step (end criterion: specific current <0.02 C). For Si||Li metal half-cells, Si thin film electrodes had an areal mass loading of 0.21 mg cm^{-2} (=0.68 mAh cm^{-2}) corresponding to a thickness of ≈900 nm. It must be noted that the low electrode mass loading may result in a small systematic mass error estimated to ≤5% for all electrodes with regard to the true Si mass loading. The WE consisted of the Si thin film (d = 12 mm), and the CE and RE were Li metal (d = 12 and 8 mm, respectively, purity: battery grade, Albemarle Corporation). A polypropylene fiber separator (Freudenberg; FS2226; three layers; d = 12.5 and 8 mm for WE/CE and RE compartments, respectively) was used to ensure sufficient wetting with GBL-based electrolytes.

For XPS, Si electrodes were lithiated in Si||Li metal pouch cells (half-cell setup, three-electrode configuration) using Si as WE (3 × 3 cm), Li metal as CE (3 × 3 cm, 50 µm thickness, Albemarle Corporation) in combination with a polypropylene separator (FS2226; 3.5 × 5 cm) and 800 µL of the respective electrolyte. Thin Nickel-stripes (Xiamen Tmax Battery Equipments Ltd.) were used as current collector contacts for both WE and CE. Tightness of pouch cells at the contact exits was ensured using pressure-sensitive self-adhesive tape (3M). A piece of Li metal pressed onto a Ni stripe served as RE, and was placed 0.5 cm apart from the aligned WE and CE on the soaked separator. Electrochemical lithiation of the Si WE was performed at 358 mA g^{-1} (0.068 mA cm^{-2}, 0.1 C, cut-off potential: 0.05 V vs Li|Li^+) followed by a constant potential step for 2 h. The extracted Si electrodes were washed with 3 × 1 mL of GBL and 2 × 1 mL of DMC.

NCM111||Si full-cells were assembled with NCM111 as the positive electrode (P) and pure or pre-lithiated Si thin films as the negative electrode (N, nomenclature according to literature).[59] The Si mass loading (0.21–0.27 mg cm^{-2}, ≈0.9–1.2 µm Si film thickness), thus, the N/P nominal capacity balancing ratio was adapted to the DoP to ensure a constant safety factor of ≈1.1–1.2 according to literature.[34] Due to a low C_{Eff} of electrolytic pre-lithiation compared to the electrochemical pre-lithiation, the N mass loading was experimentally adapted to the actual SOC of the Si electrodes after pre-lithiation, and not to the absolute pre-lithiation charge as defined for the DoP (see the subsection below).[34] NCM111||Si coin cells (CR2032, Ø = 12 mm electrodes, full-cell setup, two-electrode configuration, cell voltage control) were prepared with polypropylene membrane separators (Ø = 16 mm; Celgard 2500; Celgard) and 30 µL of 1 M $LiPF_6$/EC:EMC 3:7 +10 wt% FEC as electrolyte. To analyze individual electrode potentials, NCM111||Si pouch cells (Ø = 12 mm electrodes, full-cell setup, three-electrode configuration, cell voltage control) using polypropylene membrane separators (2 × 3 cm^2; Celgard 2500, Celgard LLC.) soaked with 120 µL of electrolyte and a Li metal-RE were assembled. The cycling procedure for full-cells consisted of three formation cycles at 0.1 C (15 mA g^{-1}; referred to NCM111; 4.2-2.5 V) including a CP step with a specific current end criterion (<0.02 C) after each half cycle (CCCV). Subsequent cycling was performed at 0.5 C (4.2–2.5 V) with a CP step after each half cycle (end criterion: specific current <0.05 C). After formation and each 50th cycle, a characterization cycle at 0.2 C followed by a 10 s discharge and charge pulse (2 C) at 50% SOC was performed for determination of the ASI.

Cell Setup for Electrolytic Pre-Lithiation: Pre-lithiation of Si electrodes via electrolysis was performed in pouch cells (half-cell setup, three-electrode configuration) using Si as a working electrode (WE; 3 × 3 cm), a coated polypropylene separator (FS2226; 3.5 × 5 cm) in combination with 800 µL of the respective electrolyte, and GCa (3 × 3 cm, HTW Germany GmbH) as CE. Al stripes (Xiamen TMax Battery Equipments Ltd.) coated with ≈50 nm of Au (DC magnetron-sputtered with the table-top sputter coater QT150ES, Quorum) were used as the current collector for the CE to minimize the possible impact of Al-dissolution. A piece of Li metal pressed onto a Ni stripe served as a reference electrode (RE), and was placed 0.5 cm apart from the aligned WE and CE on the soaked separator. It must be noted that up to 40% of the electrolyte salt was consumed upon full pre-lithiation to 0.05 V versus Li|Li^+ using the electrolysis pouch cell setup. Electrolytic pre-lithiation of Si for NCM111||Si full cells was performed at 0.1 C (358 mA g^{-1}, referred to as Si) to the specified DoP using the same setup and washing procedure as described above. The DoP was defined as pre-lithiated charge capacity relative to the nominal Si first charge, that is, first lithiation capacity (≈4000 mAh g^{-1}). After the pre-lithiation procedure, four 12 mm discs were stamped out of one 3 × 3 cm^2 Si electrode.

For the application of a pre-lithiation setup closer to a practical "electrochemical bath," electrolytic lithiation was additionally conducted in an in-house built electrolysis beaker cell containing 140 mL of the electrolyte using the same 3 × 3 cm Si WE and GCa CE as in pouch cells (for more details, refer to Supporting Information).

EIS was conducted in potentiostatic mode using a VMP3 potentiostat (BioLogic Sciences Instruments) with 10 mV amplitude (100 KHz–10 MHz) at 20 ± 0.1 °C. Prior to measurements, cells were rested for 6 h. Si samples were pre-lithiated via electrolysis to 0.05 V versus Li|Li^+ in Si||GCa pouch cells using the same setup and procedure as described above. Four disks (Ø = 12 mm) were stamped out of the pre-lithiated Si electrodes and were assembled in symmetrical Si||Si coin cells (CR2032) using polypropylene membrane separators (Celgard 2500; Celgard; 25 µm thickness, Ø = 16 mm) and 30 µL of 1 M $LiPF_6$/EC:EMC 3:7 (*w/w*) as electrolyte.

Analytical Techniques: SEM was performed to analyze electrode morphology using a Carl Zeiss AURIGA (Carls Zeiss Microscopy GmbH). Pre-lithiated Si (lithiated to 0.05 V vs Li|Li^+) was prepared as described above, and transferred into the microscope chamber via an air-tight transport vessel to prevent contact with humidity and oxygen.

XPS was performed with an Axis Ultra DLD (Kratos Analytical Ltd) to analyze the surface of lithiated Si electrodes (for preparation, see Cell Preparation and Electrochemical Measurements, Experimental

Section). Samples were analyzed with monochromatic Al K_α X-Rays ($h\nu$ = 1486 eV, 12 kV, 10 mA) using a charge neutralizer for compensation of charging. For core level spectra, a pass energy of 20 eV and a step width of 0.1 eV was set at 0° angle of emission to the surface normal. The binding energy (BE) scale was referenced to the C 1s C—H/C—C peak (BE = 284.8 eV). Measurements were conducted with samples from three independent cells to ensure reproducibility. SDP was performed using an Ar^+ ion gun (0.5 kV, 50 µA extractor current) and reproduced at least one time. Spectra are depicted without normalization, for sputter depth profiles, spectra were stacked.

ICP-OES was used to quantify the dissolution of Cu, Al, or Ni cations into the electrolyte caused by corrosion of current collectors in the electrolysis setup. Measurements were performed on Spectro Arcos (Spectro Analytical Instruments GmbH) with axial plasma viewing. For analysis, the following emission lines were observed: Cu, Ni, and Al. Parameters were set according to previously reported values.[60]

Gas chromatography-mass spectrometry (GC-MS) measurements were conducted using a GCMS-QP2010 Ultra with AOC-5000 Plus autosampler (Shimadzu, Japan) and a Supelco SLB-5 ms column (Sigma Aldrich). Sample extraction was performed via an SPME unit from CTC Analytics, Switzerland, using a polydimethylsiloxane-based fiber coated with 85 µm polyacrylate (1 cm length, Restek GmbH). Pre-concentration was performed at room temperature for 60 s. Samples were prepared by mixing electrolytes taken from ELCs with 20 wt% of VC. Further, GC and SPME parameters were applied according to reported values.[61] For detection of Cl_2 via oxidation of Br^-, 200 µL of electrolyte extracted after electrolysis was mixed with 0.5 M LiBr/acetonitrile (500 µL) and subsequently with cyclohexane (500 µL).

Supporting Information

Supporting Information is available from the Wiley Online Library or from the author.

Acknowledgements

The authors wish to thank the Federal Ministry of Education and Research (BMBF) for funding this work in the project "PräLi" (03XP0238X) within the ProZell competence cluster. Further, the authors thank Adrian Fries, Felix Dahlhaus, and the technical staff of the department of physics for help with the design and construction of the electrolysis cell. Andre Bar is acknowledged for his graphical support.

Open access funding enabled and organized by Projekt DEAL.

Conflict of Interest

The authors declare no conflict of interest.

Data Availability Statement

The data that support the findings of this study are available from the corresponding author upon reasonable request.

Keywords

anodes, electrolysis, full-cells, lithium-ion batteries, pre-lithiation, silicon, solid electrolyte interphases

Received: October 22, 2022
Revised: November 22, 2022
Published online: December 11, 2022

[1] a) Z. P. Cano, D. Banham, S. Ye, A. Hintennach, J. Lu, M. Fowler, Z. Chen, *Nat. Energy* **2018**, *3*, 279; b) E. Helmers, J. Dietz, M. Weiss, *Sustainability* **2020**, *12*, 1241; c) A. Lajunen, T. Lipman, *Energy* **2016**, *106*, 329; d) S. Dühnen, J. Betz, M. Kolek, R. Schmuch, M. Winter, T. Placke, *Small Methods* **2020**, *4*, 2070023.
[2] M. N. Obrovac, V. L. Chevrier, *Chem. Rev.* **2014**, *114*, 11444.
[3] B. Key, R. Bhattacharyya, M. Morcrette, V. Seznéc, J.-M. Tarascon, C. P. Grey, *J. Am. Chem. Soc.* **2009**, *131*, 9239.
[4] P. Bärmann, B. Krueger, S. Casino, M. Winter, T. Placke, G. Wittstock, *ACS Appl. Mater. Interfaces* **2020**, *12*, 55903.
[5] a) L. Baggetto, R. A. H. Niessen, F. Roozeboom, P. H. L. Notten, *Adv. Funct. Mater.* **2008**, *18*, 1057; b) B. Jerliu, E. Hüger, L. Dörrer, B.-K. Seidlhofer, R. Steitz, V. Oberst, U. Geckle, M. Bruns, H. Schmidt, *J. Phys. Chem. C* **2014**, *118*, 9395; c) C. Wölke, B. A. Sadeghi, G. G. Eshetu, E. Figgemeier, M. Winter, I. Cekic-Laskovic, *Adv. Mater. Interfaces* **2022**, *9*, 2101898.
[6] M. N. Obrovac, L. Christensen, *Electrochem. Solid-State Lett.* **2004**, *7*, A93.
[7] K. Ogata, E. Salager, C. J. Kerr, A. E. Fraser, C. Ducati, A. J. Morris, S. Hofmann, C. P. Grey, *Nat. Commun.* **2014**, *5*, 3217.
[8] a) H. Wu, Y. Cui, *Nano Today* **2012**, *7*, 414; b) X. H. Liu, L. Zhong, S. Huang, S. X. Mao, T. Zhu, J. Y. Huang, *ACS Nano* **2012**, *6*, 1522; c) H. Wu, G. Zheng, N. Liu, T. J. Carney, Y. Yang, Y. Cui, *Nano Lett.* **2012**, *12*, 904.
[9] C. K. Chan, R. Ruffo, S. S. Hong, Y. Cui, *J. Power Sources* **2009**, *189*, 1132.
[10] a) S. Chen, L. Shen, P. A. van Aken, J. Maier, Y. Yu, *Adv. Mater.* **2017**, *29*, 1605650; b) M. Ruttert, F. Holtstiege, J. Hüsker, M. Börner, M. Winter, T. Placke, *Beilstein J. Nanotechnol.* **2018**, *9*, 2381; c) X. Zhang, D. Wang, X. Qiu, Y. Ma, D. Kong, K. Müllen, X. Li, L. Zhi, *Nat. Commun.* **2020**, *11*, 3826; d) F. Dou, L. Shi, G. Chen, D. Zhang, *Electrochem. Energy Rev.* **2019**, *2*, 149.
[11] a) T. Kim, S. Park, S. M. Oh, *Electrochem. Commun.* **2007**, *154*, A1112; b) B. Guo, J. Shu, Z. Wang, H. Yang, L. Shi, Y. Liu, L. Chen, *Electrochem. Commun.* **2008**, *10*, 1876; c) W. Wu, M. Wang, J. Wang, C. Wang, Y. Deng, *ACS Appl. Energy Mater.* **2020**, *3*, 3884.
[12] Y. Chen, J. Qian, Y. Cao, H. Yang, X. Ai, *ACS Appl. Mater. Interfaces* **2012**, *4*, 3753.
[13] M. Ruttert, V. Siozios, M. Winter, T. Placke, *ACS Appl. Energy Mater.* **2020**, *3*, 743.
[14] a) N.-S. Choi, K. H. Yew, K. Y. Lee, M. Sung, H. Kim, S.-S. Kim, *J. Power Sources* **2006**, *161*, 1254; b) I. A. Shkrob, J. F. Wishart, D. P. Abraham, *J. Phys. Chem. C* **2015**, *119*, 14954; c) T. Jaumann, J. Balach, U. Langklotz, V. Sauchuk, M. Fritsch, A. Michaelis, V. Teltevskij, D. Mikhailova, S. Oswald, M. Klose, G. Stephani, R. Hauser, J. Eckert, L. Giebeler, *Energy Storage Mater.* **2017**, *6*, 26.
[15] R. Nölle, A. J. Achazi, P. Kaghazchi, M. Winter, T. Placke, *ACS Appl. Mater. Interfaces* **2018**, *10*, 28187.
[16] a) R. Nölle, J.-P. Schmiegel, M. Winter, T. Placke, *Chem. Mater.* **2019**, *32*, 173; b) S. S. Zhang, *J. Power Sources* **2006**, *163*, 567.
[17] a) V. L. Chevrier, L. Liu, D. B. Le, J. Lund, B. Molla, K. Reimer, L. J. Krause, L. D. Jensen, E. Figgemeier, K. W. Eberman, *J. Phys. Energy* **2014**, *161*, A783; b) H. Wu, G. Chan, J. W. Choi, I. Ryu, Y. Yao, M. T. McDowell, S. W. Lee, A. Jackson, Y. Yang, L. Hu, Y. Cui, *Nat. Nanotechnol.* **2012**, *7*, 310.
[18] F. Holtstiege, A. Wilken, M. Winter, T. Placke, *Phys. Chem. Chem. Phys.* **2017**, *19*, 25905.
[19] a) A. Heckmann, P. Meister, L.-Y. Kuo, M. Winter, P. Kaghazchi, T. Placke, *Electrochim. Acta* **2018**, *284*, 669; b) T. Placke, G. G. Eshetu, M. Winter, E. Figgemeier in *Lithium-Ion Batteries Enabled by Silicon Anodes*, (Eds.: C. Ban, K. Xu), The Institution of Engineering and Technology (IET), London, UK **2021**, pp. 349–404.
[20] F. Holtstiege, P. Bärmann, R. Nölle, M. Winter, T. Placke, *Batteries* **2018**, *4*, 4.

[21] F. Wang, B. Wang, J. Li, B. Wang, Y. Zhou, D. Wang, H. Liu, S. Dou, *ACS Nano* **2021**, *15*, 2197.
[22] a) X. Wang, C. Liu, S. Zhang, H. Wang, R. Wang, Y. Li, J. Sun, *ACS Appl. Energy Mater.* **2021**, *4*, 5246; b) D. Shanmukaraj, S. Grugeon, S. Laruelle, G. Douglade, J.-M. Tarascon, M. Armand, *Electrochem. Commun.* **2010**, *12*, 1344; c) Y. Sun, H.-W. Lee, Z. W. Seh, N. Liu, J. Sun, Y. Li, Y. Cui, *Nat. Energy* **2016**, *1*, 15008; d) J. Betz, L. Nowak, M. Winter, T. Placke, R. Schmuch, *J. Phys. Energy* **2019**, *166*, A3531.
[23] a) M. G. Scott, A. H. Whitehead, J. R. Owen, *J. Phys. Energy* **1998**, *145*, 1506; b) T. Tabuchi, H. Yasuda, M. Yamachi, *J. Power Sources* **2005**, *146*, 507.
[24] a) X. Zhang, H. Qu, W. Ji, D. Zheng, T. Ding, D. Qiu, D. Qu, *J. Power Sources* **2020**, *478*, 229067; b) J. Choi, H. Jeong, J. Jang, A.-R. Jeon, I. Kang, M. Kwon, J. Hong, M. Lee, *J. Am. Chem. Soc.* **2021**, *143*, 9169.
[25] a) C. L. Berhaut, D. Z. Dominguez, D. Tomasi, C. Vincens, C. Haon, Y. Reynier, W. Porcher, N. Boudet, N. Blanc, G. A. Chahine, S. Tardif, S. Pouget, S. Lyonnard, *Energy Storage Mater.* **2020**, *29*, 190; b) N. Liu, L. Hu, M. T. McDowell, A. Jackson, Y. Cui, *ACS Nano* **2011**, *5*, 6487.
[26] a) A. Shellikeri, V. G. Watson, D. L. Adams, E. E. Kalu, J. A. Read, T. R. Jow, J. P. Zheng, *ECS Trans.* **2017**, *77*, 293; b) P. Bärmann, M. Mohrhardt, J. E. Frerichs, M. Helling, A. Kolesnikov, S. Klabunde, S. Nowak, M. R. Hansen, M. Winter, T. Placke, *Adv. Energy Mater.* **2021**, *11*, 2100925.
[27] C. R. Jarvis, M. J. Lain, M. V. Yakovleva, Y. Gao, *J. Power Sources* **2006**, *162*, 800.
[28] E. Adhitama, F. D. Brandao, I. Dienwiebel, M. M. Bela, A. Javed, L. Haneke, M. C. Stan, M. Winter, A. Gomez-Martin, T. Placke, *Adv. Funct. Mater.* **2022**, *32*, 2201455.
[29] H. J. Kim, S. Choi, S. J. Lee, M. W. Seo, J. G. Lee, E. Deniz, Y. J. Lee, E. K. Kim, J. W. Choi, *Nano Lett.* **2016**, *16*, 282.
[30] a) T. Tsuda, N. Ando, N. Mitsuhashi, T. Tanabe, K. Itagaki, N. Soma, S. Nakamura, N. Hayashi, F. Matsumoto, *ECS Trans.* **2017**, *77*, 1897; b) M. Arnaiz, J. Ajuria, *Batteries Supercaps* **2021**, *4*, 733.
[31] H. Zhou, X. Wang, D. Chen, *ChemSusChem* **2015**, *8*, 2737.
[32] a) R. W. Grant, M. Sweetland, A. M. Acharige, (Nanoscale Components, *Inc.*), US 9,598,789 B2 **2017**; b) R. W. Grant, M. Sweetland, A. M. Acharige, (Nanoscale Components, *Inc.*), US 20,170,187,030 A1 **2017**.
[33] R. W. Grant, M. Sweetland, A. M. Acharige, R. Wohl, (Nanoscale Components, *Inc.*), US 9,748,599 B2 **2017**.
[34] V. L. Chevrier, L. Liu, R. Wohl, A. Chandrasoma, J. A. Vega, K. W. Eberman, P. Stegmaier, E. Figgemeier, *J. Electrochem. Soc.* **2018**, *165*, A1129.
[35] M.-T. F. Rodrigues, J. A. Gilbert, K. Kalaga, D. P. Abraham, *J. Phys. Energy* **2020**, *2*, 24002.
[36] a) R. W. Schmitz, P. Murmann, R. Schmitz, R. Müller, L. Krämer, J. Kasnatscheew, P. Isken, P. Niehoff, S. Nowak, G.-V. Röschenthaler, N. Ignatiev, P. Sartori, S. Passerini, M. Kunze, A. Lex-Balducci, C. Schreiner, I. Cekic-Laskovic, M. Winter, *Prog. Solid State Chem.* **2014**, *42*, 65; b) M. L. Lazar, B. L. Lucht, *J. Phys. Energy* **2015**, *162*, A928.
[37] a) L. J. Krause, V. L. Chevrier, L. D. Jensen, T. Brandt, *J. Phys. Energy* **2017**, *164*, A2527; b) D. Aurbach, Y. Gofer, M. Ben-Zion, P. Aped, *J. Electroanal. Chem.* **1992**, *339*, 451.
[38] K. Xu, U. Lee, S. Zhang, M. Wood, T. R. Jow, *Electrochem. Solid-State Lett.* **2003**, *6*, A144.
[39] A. Xiao, L. Yang, B. L. Lucht, S.-H. Kang, D. P. Abraham, *J. Phys. Energy* **2009**, *156*, A318.
[40] N.-S. Choi, K. H. Yew, H. Kim, S.-S. Kim, W.-U. Choi, *J. Power Sources* **2007**, *172*, 404.
[41] a) V. Etacheri, O. Haik, Y. Goffer, G. A. Roberts, I. C. Stefan, R. Fasching, D. Aurbach, *Langmuir* **2012**, *28*, 965; b) Y. Stenzel, F. Horsthemke, M. Winter, S. Nowak, *Separations* **2019**, *6*, 26; c) J. Henschel, C. Peschel, S. Klein, F. Horsthemke, M. Winter, S. Nowak, *Angew. Chem., Int. Ed.* **2020**, *59*, 6128.
[42] M. Lanz, P. Novák, *J. Power Sources* **2001**, *102*, 277.
[43] I. A. Shkrob, Y. Zhu, T. W. Marin, D. P. Abraham, *J. Phys. Chem. C* **2013**, *117*, 23750.
[44] S. Jurng, Z. L. Brown, J. Kim, B. L. Lucht, *Energy Environ. Sci.* **2018**, *11*, 2600.
[45] S. Huang, S. Wang, G. Hu, L.-Z. Cheong, C. Shen, *Appl. Surf. Sci.* **2018**, *441*, 265.
[46] R. I. R. Blyth, H. Buqa, F. P. Netzer, M. G. Ramsey, J. O. Besenhard, P. Golob, M. Winter, *Appl. Surf. Sci.* **2000**, *167*, 99.
[47] R. Dedryvère, S. Leroy, H. Martinez, F. Blanchard, D. Lemordant, D. Gonbeau, *J. Phys. Chem. B* **2006**, *110*, 12986.
[48] Y. Xie, P. M. A. Sherwood, *Appl. Spectrosc.* **1990**, *44*, 797.
[49] a) R. Dedryvère, L. Gireaud, S. Grugeon, S. Laruelle, J.-M. Tarascon, D. Gonbeau, *J. Phys. Chem. B* **2005**, *109*, 15868; b) A. M. Andersson, K. Edström, *J. Power Sources* **2001**, *148*, A1100; c) S. Chenakin, N. Kruse, *J. Phys. Chem. C* **2019**, *123*, 30926.
[50] D. Aurbach, *J. Phys. Energy* **1989**, *136*, 1606.
[51] K. U. Schwenke, S. Solchenbach, J. Demeaux, B. L. Lucht, H. A. Gasteiger, *J. Phys. Energy* **2019**, *166*, A2035.
[52] B. Philippe, R. Dedryvère, J. Allouche, F. Lindgren, M. Gorgoi, H. Rensmo, D. Gonbeau, K. Edström, *Chem. Mater.* **2012**, *24*, 1107.
[53] a) K. Edström, M. Herstedt, D. P. Abraham, *J. Power Sources* **2006**, *153*, 380; b) A. M. Andersson, A. Henningson, H. Siegbahn, U. Jansson, K. Edström, *J. Power Sources* **2003**, *119*, 522; c) P. Niehoff, S. Passerini, M. Winter, *Langmuir* **2013**, *29*, 5806; d) T. Nobuta, T. Ogawa, *J. Mater. Sci.* **2009**, *44*, 1800.
[54] J. Graetz, C. C. Ahn, R. Yazami, B. Fultz, *Electrochem. Solid-State Lett.* **2003**, *6*, A194.
[55] L. Hanf, M. Diehl, L.-S. Kemper, M. Winter, S. Nowak, *Electrophoresis* **2020**, *41*, 1568.
[56] D. Pritzl, J. Landesfeind, S. Solchenbach, H. A. Gasteiger, *J. Phys. Energy* **2018**, *165*, A2145.
[57] a) C. Hitz, A. Lasia, *J. Electroanal. Chem.* **2001**, *500*, 213; b) J.-P. Diard, B. Le Gorrec, C. Montella, *J. Electroanal. Chem.* **1999**, *471*, 126.
[58] Y. M. Lee, J. Y. Lee, H.-T. Shim, J. K. Lee, J.-K. Park, *J. Electrochem. Soc.* **2007**, *154*, A515.
[59] R. Nölle, K. Beltrop, F. Holtstiege, J. Kasnatscheew, T. Placke, M. Winter, *Mater. Today* **2020**, *32*, 131.
[60] M. Evertz, J. Kasnatscheew, M. Winter, S. Nowak, *Anal. Bioanal. Chem.* **2019**, *411*, 277.
[61] F. Horsthemke, A. Friesen, X. Mönnighoff, Y. P. Stenzel, M. Grützke, J. T. Andersson, M. Winter, S. Nowak, *RSC Adv.* **2017**, *7*, 46989.